Journal of Hazardous Materials 189 (2011) 595–602

Contents lists available at ScienceDirect

Journal of Hazardous Materials

journal homepage: www.elsevier.com/locate/jhazmat

Increasing the catalytic activities of iodine doped titanium dioxide by modifying with tin dioxide for the photodegradation of 2-chlorophenol under visible light irradiation

Zhiqiao He [a], Cheng Wang [a], Hongyu Wang [b], Fangyue Hong [a], Xinhua Xu [c], Jianmeng Chen [a], Shuang Song [a,*]

[a] College of Biological and Environmental Engineering, Zhejiang University of Technology, Hangzhou 310032, PR China
[b] College of Civil Engineering and Architecture, Zhejiang University of Technology, Hangzhou 310032, PR China
[c] College of Environmental and Resource Sciences, Zhejiang University, Hangzhou 310029, PR China

ARTICLE INFO

Article history:
Received 1 November 2010
Received in revised form 24 February 2011
Accepted 24 February 2011
Available online 2 March 2011

Keywords:
TiO_2
SnO_2
Iodine
Photocatalysis
2-Chlorophenol

ABSTRACT

The photocatalytic degradation of 2-chlorophenol (2-CP) irradiated with visible light over iodine doped TiO_2 (IT) modified with SnO_2 (SIT) nanoparticles has been investigated in this study. The structure and optical properties of the SIT catalysts have been well characterized by X-ray diffraction, the Brunauer–Emmett–Teller method, transmission electron microscopy, UV–visible absorption spectra and X-ray photoelectron spectroscopy. The effects of preparation conditions, such as SnO_2 content and calcination temperature, on the photocatalytic degradation efficiency have been surveyed in detail. The improved photocatalytic activity of SIT is derived from the synergistic effect between the SnO_2 and IT, which promoted the efficiency of migration of the photogenerated carriers at the interface of the catalysts and thereby enhanced the efficiency of photon harvesting in the visible region. The action of scavengers (fluoride ion, iodide ion, *tert*-butyl alcohol, and persulfate ion), as well as N_2 purging on the photodegradation rate reveal that the valence band hole is mainly responsible for the effective photocatalytic removal of 2-CP and the corresponding TOC reduction.

1. Introduction

The semiconductor photocatalysts have attracted great interest over the past decade because of their unusual optical and electrical properties and their application as alternatives for hydrogen generation and air purification, as well as water disinfection and purification [1–4]. Among various oxide semiconductor photocatalysts, titanium dioxide (TiO_2) nanostructures are recognized to be the most suitable candidates for widespread applications in environmental purification and remediation [1,3,4], owing to their biological and chemical inertness, high photocatalytic efficiency, low cost, and photostability against photocorrosion and chemical corrosion. Unfortunately, the photocatalytic activity (PA) of TiO_2 has been largely limited to the UV light region, using approximately 5% of the sunlight available [5,6]. Therefore, considerable effort needs to be made to modify the TiO_2 materials in order to broaden the photoresponse to longer wavelength.

The photocatalytic process originates from the generation of charge carriers under light irradiation, producing electrons and holes in the conduction band (CB) and valence band (VB), as a result of photoexcitation of TiO_2. Those holes diffuse to the TiO_2 surface and react with pre-adsorbed H_2O/OH^- to yield $HO^\bullet$. Oxygen can act as an electron acceptor to produce superoxide radical ions ($O_2^{-\bullet}$), which are spontaneously transformed to H_2O_2 and $HO^\bullet$ [7–10]. Both active $HO^\bullet$ and $O_2^{-\bullet}$ are considered as the major oxidants in the photocatalytic degradation. Nevertheless, a high e^-–h^+ recombination rate (~10 ns) certainly reduces the quantum efficiency and represents the major drawback for applications using TiO_2 [8–10]. Hence, considerable attention has been paid to decreasing the recombination rate of electron–hole pairs so as to achieve good photocatalytic performance.

Recently, a novel class of visible-light-activated iodine-doped TiO_2 photocatalyst (IT) has been reported by some groups, which might enhance the PA of TiO_2 under visible or UV–visible light irradiation [11–14]. Earlier studies asserted that the iodine in TiO_2 is in the form of negatively charged iodine (I^-) and heptavalent iodine (I^{7+}) species produced via the disproportionation of IO_3^- ($4IO_3^- \rightarrow 3IO_4^- + I^-$). Since the ionic radius of I^- (0.216 nm) is much larger than that of O^{2-} (0.124 nm) or Ti^{4+} (0.068 nm), substitution of Ti^{4+} or O^{2-} in the lattice with the IO_4^-/I^- species does not occur, as concluded by Su et al. [14]. Nevertheless, there are conflicting accounts of the form of the doped iodine ion. Some researchers

* Corresponding author. Tel.: +86 571 88320726; fax: +86 571 88320276.
E-mail address: ss@zjut.edu.cn (S. Song).

0304-3894/$ – see front matter © 2011 Elsevier B.V. All rights reserved.
doi:10.1016/j.jhazmat.2011.02.077

propose that the iodine exists mainly as I^{5+} in the TiO_2 lattice precisely because of similarity of its ionic radius [11,13]. Liu et al. had reported that the coexistence of I–O–I and I–O–Ti structures can change the surface structure on account of the release of local strain energies, which are responsible for the wider range visible light response exhibited in anatase TiO_2 [15]. In any case, doped iodine can show stronger absorption, with a red shift in the band gap transition and higher PA than pure TiO_2 or P25 [11–15].

Furthermore, if TiO_2 is mixed with another semiconductor whose CB is at a lower potential than TiO_2, the electrons present in the CB of TiO_2 can be transferred to the second semiconductor and the recombination rate comes down [16]. The TiO_2–SnO_2 system seems to be the pair of choice because of the structural analogy between both oxides. Though the band gap of TiO_2 (3.2 eV) is lower than that of SnO_2 (3.8 eV), the CB edge of TiO_2 (E_{CB} = 0 V versus NHE at pH 7.0) is above the CB edge of SnO_2 (E_{CB} = −0.5 V versus NHE at pH 7.0) [16–21]. The CB of SnO_2 acts as a sink for photogenerated electrons transferring from TiO_2 to SnO_2, helping the photogenerated holes to move in the opposite direction to escape recombination with each other, and thereby increasing the efficiency of charge separation [19].

To the best of our knowledge, there is a systematic discrepancy in the description of the synergistic effect of the IT catalyst and tin oxide on the degradation of pollutants under visible-light irradiation. In this work, a new type of TiO_2 photocatalyst, IT modified with SnO_2 (SIT), has been synthesized and characterized by X-ray diffraction (XRD), Brunauer–Emmett–Teller (BET), transmission electron microscopy (TEM), UV–visible absorption spectra and X-ray photoelectron spectroscopy (XPS) analysis. The effect of SnO_2 on the IT of the catalyst, evaluated using the photodegradation of 2-chlorophenol (2-CP) as a probe reaction under irradiation with visible light, is correlated with the calcination temperature and the molar ratio of Sn/Ti. Finally, we discuss the possible active species in the photocatalytic systems studied using several scavengers and N_2 purging.

In the past few years, photocatalytic degradation of 2-CP has been carried out over various TiO_2 based catalysts [22–27]. 2-CP was chosen as model target pollutant because it is widely used in industry and daily life, and have caused considerable damage and threat to the aquatic ecosystem and human health [22,28].

2. Experimental

2.1. Materials

All chemicals were of analytical grade or higher and were used as received. Iodic acid (HIO_3), tin chloride ($SnCl_4$), tetrabutyl titanate ($Ti(BuO)_4$), and *n*-butyl alcohol (C_4H_9OH) as the starting materials were obtained from Huadong Medicine Co., China. Sodium nitrite ($NaNO_2$) and 2-CP were purchased from Shanghai Jingchun Reagent Co., China. Potassium iodide (KI), *tert*-butyl alcohol (*t*-BuOH), sodium fluoride (NaF), and potassium persulfate ($K_2S_2O_8$) used as scavengers were supplied by Huadong Medicine Co., Ltd., China. Nitrogen (purity 99.99%) was provided by Hangzhou Jingong Special Gas Co., Ltd., China. Deionized water (18 MΩ) was used for all solutions.

2.2. Synthesis of catalysts

The photocatalyst precursor solution was synthesized by means of a hydrolysis method as follows: 7.5 mmol of $SnCl_4$ source was added to 35 mL of C_4H_9OH and then mixed with 51 mL of $Ti(BuO)_4$. Later, the solution was added dropwise to 200 mL of 30 mM aqueous iodic acid under magnetic stirring. After heating at 80 °C for 16 h in a temperature-controlled bath, the color of the mixture turned to yellow. Subsequently, the powder was dried in a vacuum oven (DZG-6050SA, Shanghai Sumsung Laboratory Instrument Co., Ltd, China) at a temperature of 80 °C and a vacuum pressure of 0.1 MPa. Finally, the resulting dry powders were calcined in an oven (CWF1100, Carbolite, UK) at a rate of 5 °C min^{-1} to 400 °C and held at this temperature for 2 h, followed by cooling to room temperature naturally. The final samples were used for the PA test and characterization.

A series of samples was synthesized in the same way by changing the concentrations of $SnCl_4$ and the calcination temperatures. The catalysts are denoted as SIT_A-*B*, where A denotes the molar ratio of Sn/Ti, expressed as a percentage, and *B* represents the calcination temperature (°C). 5% SnO_2 on TiO_2 (ST_5) and IT were used for control experiments.

2.3. Catalysts characterization

To determine the crystal phase and the crystallite size of the photocatalysts, powder XRD patterns of these samples were recorded using a Thermo ARL SCINTAG X'TRA diffractometer with Cu Kα radiation. The accelerating voltage and emission current were 45 kV and 40 mA, respectively. The crystal phases were identified by comparison with JCPDS cards and the crystallite sizes were calculated by X-ray line broadening analysis according to the Debye–Scherrer formula.

Specific surface areas (S_{BET}) of the samples were performed using the BET method with a Micromeritics ASAP 2010 analyser by measurement of the nitrogen adsorption–desorption isotherm at 77 K. The Barret–Joyner–Halenda (BJH) method was used to obtain pore size distribution of the samples.

TEM images were recorded by ultrasonically dispersing the powders in water prior to deposition on a carbon-coated TEM grid and obtained on a JEOL-2010 microscope operating at an accelerating voltage of 200 kV with a 0.19-nm point resolution.

UV–visible absorption spectra of samples were determined at room temperature on a Spectro UV-2550 instrument equipped with an integrating sphere accessory. $BaSO_4$ was used as a standard white board.

XPS examination was carried out on an RBD upgraded PHI-5000C ESCA system (Perkin–Elmer) with Mg KR radiation (1253.6 eV). All the binding energies were referenced to the C1s peak at 284.6 eV of the surface adventitious carbon. Data were analyzed using XPSPEAK4.1 software provided by Raymund W.M. Kwok (The Chinese University of Hong Kong, China).

2.4. Photochemical experiments

Photocatalytic experiments were carried out in a cylindrical Pyrex photoreactor (diameter 16 cm, height 20 cm). The cylindrical reactor consisted of three parts. From inside to outside, the first part is a 1000-mL water filter containing 2 M sodium nitrite hung with a 400-W dysprosium lamp (Beijing Electric Light Sources Research Institute, Beijing, China) with a similar spectrum to that of the sun. The second part is an outside photoreactor with running water passing through it to cool the reaction solution using a thermostat (THD-2015, Tianheng Instrument Factory, Ningbo, China). Owing to the continuous cooling, the temperature of the reaction solution is maintained at approximately 22 °C and that of the filter solution at 55 °C. At the start of the experiment, the reaction solution containing 1.5 L of aqueous suspension with 0.25 mM 2-CP and 1.5 g of catalyst is put in the reactor. The third part is a water-jacketed reactor. For purging nitrogen gas experiments, cylindrical nitrogen gas diffusers with coarse porosity were placed at the bottom of the reactor. Nitrogen gas at a flow rate of 0.08 m^3 h^{-1}, controlled by a rotameter, was used to give the desired oxygen level.

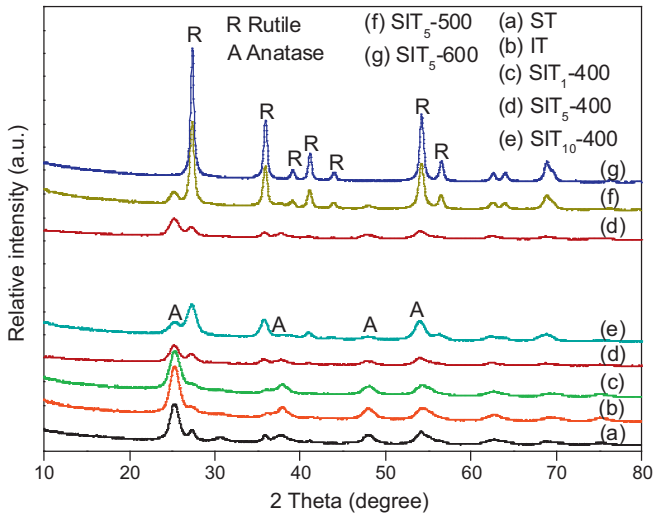

Fig. 1. XRD patterns of ST_5, IT, SIT_1-400, SIT_5-400, SIT_{10}-400, SIT_5-500 and SIT_5-600.

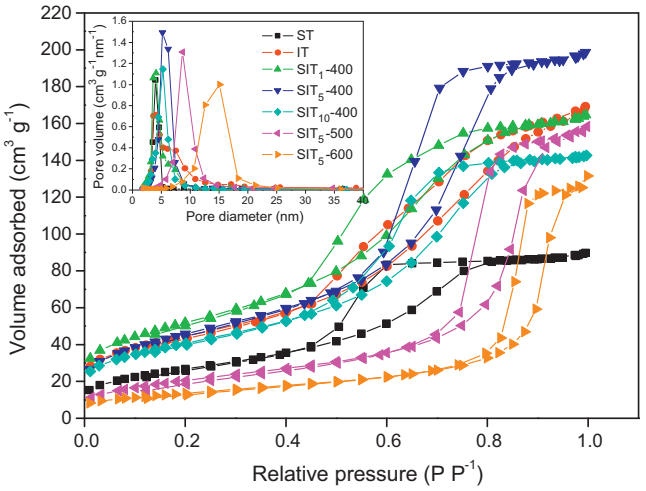

Fig. 2. Nitrogen adsorption–desorption isotherms and pore size distribution (inset) of ST_5, IT, SIT_1-400, SIT_5-400, SIT_{10}-400, SIT_5-500 and SIT_5-600.

During each run, 5 mL samples were withdrawn at predetermined intervals and then centrifuged and filtered through a hypodermic syringe fitted with a 0.45 μm Millipore filter to remove the catalyst particles. Quantitative analysis of 2-CP were evaluated by the Agilent 1200 Series high-pressure liquid chromatography (HPLC) equipped with an Agilent ZORBAX SB-C18 column (4.6 mm × 250 mm, 5 μm). 5 μL samples were injected on to the column to determine the concentration of 2-CP. The flow rate was 0.8 mL min^{-1} and the detection wavelength was 280 nm, using methanol/water (70:30, v/v) as the mobile phase.

Identification of the extent of mineralization was performed to monitor TOC changes during photocatalysis by a total organic carbon analyzer (TOC-V_{CPH}; Shimadzu, Japan).

3. Results and discussion

3.1. Catalyst characterization

XRD is an effective method for identifying the phases. The effects of the molar ratios of Sn/Ti and the calcination temperature on the phase structure and composition are illustrated in Fig. 1. All the peaks observed can be assigned to anatase (JCPDS card no. 21-1272) and rutile (JCPDS card no. 21-1276) phases. Unfortunately, no separate discernible phases corresponding to SnO_2 are seen. The relative intensities of the anatase and rutile diffraction peaks are different for the samples obtained with different molar ratios of Sn/Ti and different calcination temperatures. The mass fraction of rutile (W_R) in the samples can be calculated by measuring the intensities of the strongest (1 1 0) and (1 0 1) diffraction peaks of rutile (I_R) and anatase (I_A), respectively [12,29].

$$W_R = \frac{I_R}{0.886 I_A + I_R}$$

It can be seen from Table 1 and Fig. 1 that the intensity of peaks assigned to the rutile phase increased with SnO_2 concentration, suggesting that SnO_2 can promote the appearance of the TiO_2 rutile phase and inhibit the formation of the anatase phase. This is in agreement with results reported previously [16,17,19]. During the preparation of the catalyst particles, the nucleation barrier of the SIT is reduced by the presence of SnO_2 grains, and the overgrowth of crystalline TiO_2 immediately occurs near the rutile SnO_2, leading to the generation of TiO_2 rutile phase rather than anatase [30].

On the other hand, the increased calcination temperature can induce a phase transformation from anatase to rutile and accelerate the growth of crystallites [29]. When the calcination temperature increases to 500 °C, a progressive increase in the rutile phase occurs, as indicated by the characteristic diffraction peaks centered at 27.4° (1 1 0). With further increase of the calcination temperature to 600 °C, the anatase phase disappears and completely transforms to the rutile phase.

As estimated from the Debye–Scherrer equation (Table 1), the crystallite sizes calculated from the XRD peaks of the crystal plane (1 0 1) in anatase were 7.2 nm, 6.6 nm, 6.3 nm, 6.5 nm, 6.4 nm, and 8.1 nm for ST_5, IT, SIT_1-400, SIT_5-400, SIT_{10}-400 nm and SIT_5-500, respectively. Clearly, the addition of Sn reduced the crystal size of the IT grains. The introduction of tin ions changes the surface charge of the particles, separating them from each other and thereby reducing the growth rate of the TiO_2 sol particles. In other words, the dopant SnO_2 can inhibit grain growth by restricting the coalescence of some smaller neighboring grains. Therefore, smaller size particles are most likely to be formed, as compared with IT [31]. Furthermore, the crystallite sizes of the photocatalyst increases with increasing sintering temperatures. Particles sintered at higher temperature have high surface energy, and thus the particles are less stable and can agglomerate to form larger particles.

The nitrogen adsorption–desorption isotherms and the corresponding pore size distribution were measured to indicate the S_{BET} and pore structure of the resultant catalysts. According to the 1985 IUPAC classification [32], the results in Fig. 2 show that all samples except ST_5 are typical of a Type IV isotherm, which is characteristic of mesoporous materials. Also, the hysteresis loops are a signature of capillary condensation. By comparison, the ST_5 sample forms an open capillary of ink bottle shapes accounting for the hysteresis in the adsorption–desorption isotherms [33].

S_{BET}, average pore diameter, and pore volume of the samples are summarized in Table 1. Generally, the S_{BET} of SIT_1-400, SIT_5-400 and SIT_{10}-400 are higher than those of ST_5 and IT calcined at 400 °C. This is reasonable because the smaller crystal size usually shows the higher surface area. Nonetheless, The S_{BET} decreases gradually with the SnO_2 concentration increasing from 1% to 10%, indicating that the SnO_2 coverage of IT becomes higher, blocking the pores of the IT [19]. At the same time, the data in Table 1 and Fig. 2 show that S_{BET} and the peak of pore volume distribution curves decrease sharply with the increase of calcination temperature, due to crystallite growth or sintering [34].

TEM can directly image the structure of the material. Hence, TEM observations were used to judge the crystalline structure and particle size of the SIT_5-400 composite powder. The results are shown in

Table 1
Refined physicochemical parameters for the prepared catalysts.

Samples	S_{BET} ($m^2\ g^{-1}$)	Crystalline phases (%)[a]	Crystal size (nm)	Pore diameter (nm)	Pore volume ($cm^3\ g^{-1}$)	Indirect band gap (eV)
ST_5	97.7	A82, R18	7.2	5.69	0.14	2.75
IT	159.9	A90, R10	6.6	6.54	0.26	2.71
SIT_1-400	186.7	A90, R10	6.3	5.46	0.25	2.52
SIT_5-400	167.2	A65, R35	6.5	7.35	0.31	2.43
SIT_{10}-400	146.7	A30, R70	6.4	6.02	0.22	2.25
SIT_5-500	77.2	A18, R82	8.1	12.7	0.24	2.54
SIT_5-600	49.4	R100	–	16.5	0.20	2.69

[a] A and R denotes Anatase and Rutile, respectively.

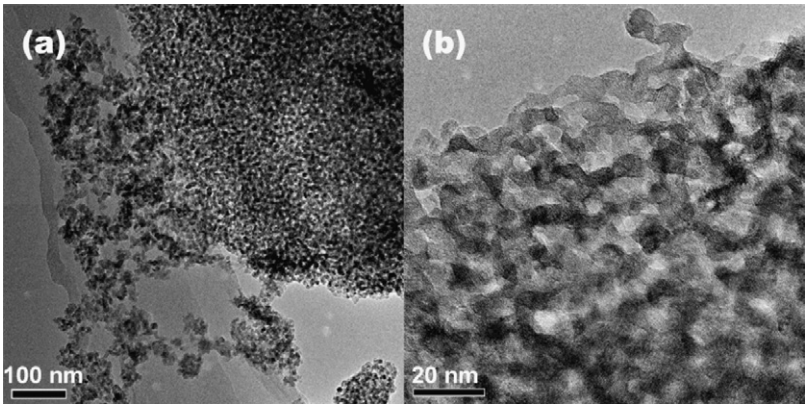

Fig. 3. TEM images of SIT_5-400.

Fig. 3. The SIT_5-400 sample has a honeycomb porous structure with fine particulate morphology, partly originating from inter-particle porosity. The average particle size of SIT_5-400 observed by TEM images is ~7 nm, almost the same as the crystallite sizes calculated by the Debye–Scherrer equation.

UV–visible absorption spectra is a particularly suitable technique to diagnose the band structure in the materials. Fig. 4 and Table 1 present the optical properties and band gaps of the catalysts. The spectrum of ST_5 and IT powders synthesized in this work are also shown for comparison. All modified TiO_2 powders have an absorption edge that stretches into the visible region. The reason for the absorption wavelength range red shifts of the ST_5 can probably be attributed to the partial phase transformation of TiO_2 from anatase to rutile [29]. The absorption measurements of IT sample show dramatic and strong photo absorption. The coexistence of I–O–I and I–O–Ti structures may account for the wider range visible light response [15]. Thus, the absorption spectrum in the range of wavelengths from 490 to 550 nm for SIT_1-400, SIT_5-400, and SIT_{10}-400 catalysts indicates that the visible light absorption is not only due to the phase transformations but also the presence of the I–O–I and I–O–Ti structures. In addition, the growth temperature also affects the band gap of these particles. The band gap increases from 2.43 eV to 2.69 eV with increase in growth temperature from 400 °C to 600 °C.

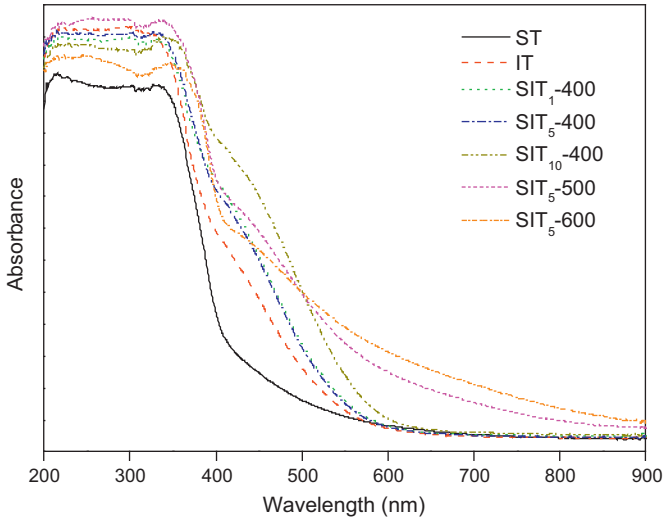

Fig. 4. UV–visible absorption spectra of ST_5, IT, SIT_1-400, SIT_5-400, SIT_{10}-400, SIT_5-500 and SIT_5-600.

The XPS technique was employed to obtain a better understanding of the chemical state of tin, iodine, and titanium atoms on the catalysts surface. Fig. 5a shows wide-scan XPS spectra of the IT and SIT_5-400. The element C may originate from non-hydrolyzed alkoxy groups, residual carbon from the precursor solution, or adventitious hydrocarbons from XPS itself. The Sn 3d, Ti $2p_{3/2}$, and I 3d5 were taken before and after all regions were scanned and the shape and intensity were consistent within approximately 1% and the binding energies were reproducible to within ±0.05 eV.

The Sn $3d_{5/2}$ and Sn $3d_{3/2}$ XPS spectrum is revealed in Fig. 5b. The Sn $3d_{5/2}$ has a binding energy of 486.0 eV and the binding energy of the Sn $3d_{3/2}$ was 494.2 eV which is in agreement with other data [35]. A closer look at the Sn $3d_{5/2}$ shows no shoulder or split peak and a small full width half maximum indicating high quality SnO_2 (one component only). The atomic percent determined from the XPS analysis for SIT_5-400 shows carbon 25.5%, oxygen 53.0%, titanium 18.4%, iodine 1.8% and tin 1.3%. The Sn/Ti ratio on the surface (~7%) is greater than 5%, illustrating that Sn is uniformly dispersed on the TiO_2 surface, since the XPS analysis is surface sensitive [5].

Fig. 5c exhibits signals obtained for the Ti $2p_{3/2}$ levels, suggesting the existence of Ti^{3+} in addition to Ti^{4+} in the Ti $2p_{3/2}$ region. The $Ti^{3+}/(Ti^{3+}+Ti^{4+})$ ratio of SIT_5-400 (34.2%) is almost the same as that of the IT sample (33.9%), certifying that Sn plays an insignificant role in the production of Ti^{3+}.

The I $3d_{5/2}$ core-level spectra for IT and SIT_5-400 are presented in Fig. 5d. Both samples exhibit two prominent peaks, at ~620

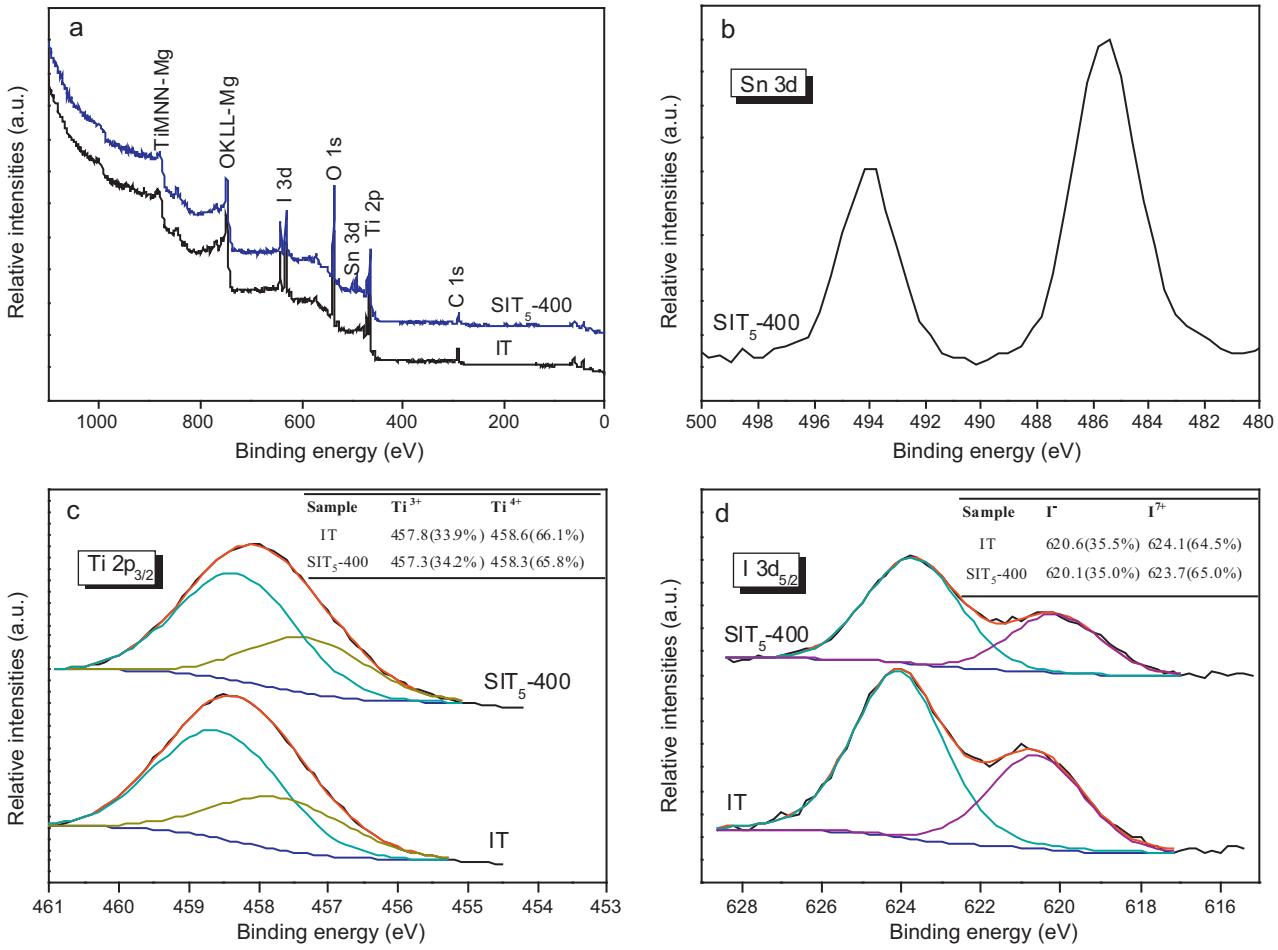

Fig. 5. XPS spectra of IT and SIT_5-400 (a), as well as XPS spectra in the core levels of Sn 3d (b), Ti $2p_{3/2}$ (c) and I $3d_{5/2}$ (d).

and ~624 eV, assigned to the negatively charged iodine (I^-) and heptavalent iodine (I^{7+}) species. Note that the surface Sn/I ratio detected by XPS is ~72%, which is significantly larger than the original (25%), corroborating the existence of Sn on the surface of IT.

3.2. Photocatalytic activity

To benchmark the PA of ST_5, IT, SIT_1-400, SIT_5-400, SIT_{10}-400, SIT_5-500, SIT_5-600, a series of experiments was conducted under visible light irradiation to investigate the photocatalytic removal of 2-CP and the corresponding TOC reduction (Fig. 6). Before heterogeneous photocatalytic experiments were performed, direct photolysis of 2-CP without a catalyst and adsorption of 2-CP on SIT_5-400 catalyst were carried out to examine their effects on the degradation of 2-CP. The results proved that ~4% of the 2-CP initially introduced was adsorbed and the direct photolysis of 2-CP was negligible.

As shown in Fig. 6a, the activity of the catalysts under visible light irradiation depended on the doping level and temperature. Typically, the SIT_5-400 showed the highest photoactivity with ~88% of 2-CP removal, with only ~48% and ~72% for ST_5 and IT, respectively. The TOC reduction rate exhibited a similar trend to that of 2-CP removal.

The SnO_2 content can influence the thickness of the superficial space-charge layer of IT. Only when the space-charge layer thickness approximates the penetration depth of light into the particle, can the electron–hole pairs be effectively separated [36]. The enhanced activity of the SIT_5-400 sample is attributed to the

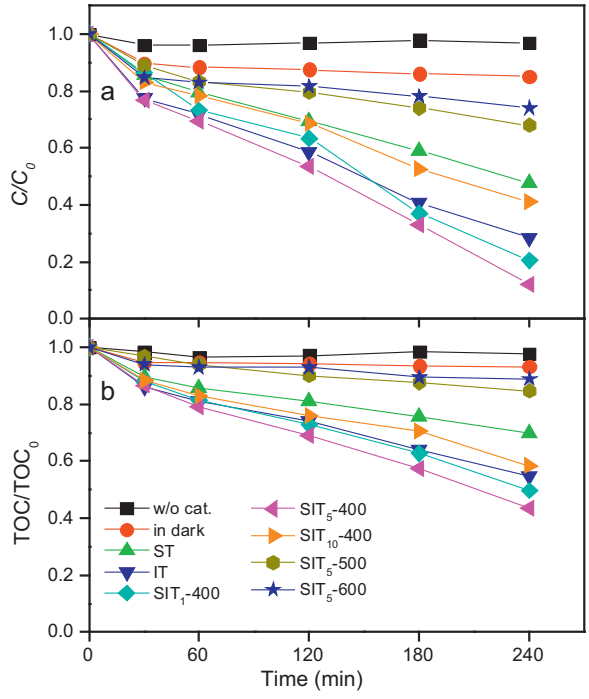

Fig. 6. Comparison of the 2-CP removal (a) and TOC reduction (b) in the presence and absence of various photocatalysts under visible light irradiation or in the presence of SIT_5-400 in the dark: initial 2-CP concentration, 0.25 mM; catalyst dosage, 1.0 g L^{-1}; reaction temperature, 22 °C.

efficient charge separation from IT to SnO_2 because of the high dispersion of SnO_2 on IT. Since SnO_2 is highly dispersed, both SnO_2 and IT nanoparticles are in close contact with each other, which has a profound influence on the transport mechanism of electrons and holes [17]. The excited electrons and holes quickly move in opposite directions to accumulate on the SnO_2 and IT particles, respectively, and hence their recombination is greatly retarded [20]. In the case when the SnO_2 content is too small (1 mol%), the high recombination rate of electron–hole pairs is due to the absence of adequate traps. In contrast, when the doping quantity is very high (10 mol%), the absorption of light and generation of electrons–holes is reduced. These analyses are consistent with the photocatalytic reduction activity of the photocatalysts with visible light illumination.

The SIT_5-500 and SIT_5-600 particles had poorer photoactivity compared with SIT_5-400. This indicates that the calcination temperature has a great effect on the PA. The characteristic results revealed that the rutile phase intensity and grain size increased with the calcination temperature, while the surface area gave opposite effects. Hence, we speculate that rutile is less favorable for PA, whereas larger specific surface areas achieve better photoactivity [30,37–40].

3.3. Dominant reactants during the degradation of 2-CP

To scrutinize the main oxidant in our photocatalytic system, we investigated the effects of NaF, KI, *t*-BuOH, dissolved oxygen and $K_2S_2O_8$ in the SIT_5-400 suspensions on 2-CP degradation irradiated by visible light.

Fluoride can be adsorbed on to the surface of TiO_2 catalysts to form the F–Ti bond [41–43]. Thus, the addition of excess NaF largely prevents the adhesion of 2-CP on the surface of the catalysts, and the formation of precursor complexes between catalysts and 2-CP is restrained [41]. Comparison of the curves in Fig. 7 indicate that the NaF had a potential inhibitory effect on 2-CP degradation with SIT_5-400 catalyst, indicating that the removal of 2-CP is mainly a surface charge process. In other words, 2-CP is preferentially adsorbed on to the active sites of catalysts before photodegradation. Because the 2-CP removal is the precondition for the whole process of photodegradation, the mineralization rate was correspondingly slow [44].

Iodide ion is an excellent scavenger, which easily captures VB hole and superficial HO• [45,46], reducing the available oxidizing species on the catalyst surface for reacting with 2-CP. In aqueous solution, the KI ionizes into iodide ions (I^-) and potassium ions (K^+). The following reaction pathway may occur, initiated by the oxidation of valence-band holes [45]:

$$I^- \leftrightarrow I^\bullet + e^-$$

$$I^\bullet + I^- \rightarrow I_2^{\bullet -}$$

$$I_2^{\bullet -} \leftrightarrow I_2 + e^-$$

The I_2 aqueous solution displayed absorption below 690 nm, with two prominent absorption peaks at 287 nm and 353 nm, as determined by a UV–visible spectrophotometer. Hence, the quantitative determination of 2-CP by HPLC was interfered with after the addition of KI. Thus TOC reduction was selected as the target value to match against the actual results. When 2.5 mM KI was used as a diagnostic tool for suppressing the hole process and reducing superficial HO•, the TOC reduction of 2-CP was significantly inhibited. Accordingly, the 2-CP degradation is caused chiefly by the action of h_{vb}^+ and/or superficial HO•.

The t-BuOH, a known HO• scavenger with a reaction rate constant of $6.0 \times 10^8\ M^{-1}\ s^{-1}$, will cause a great decrease in the reaction rate if the mechanism is controlled by HO• [44]. As shown in Fig. 7,

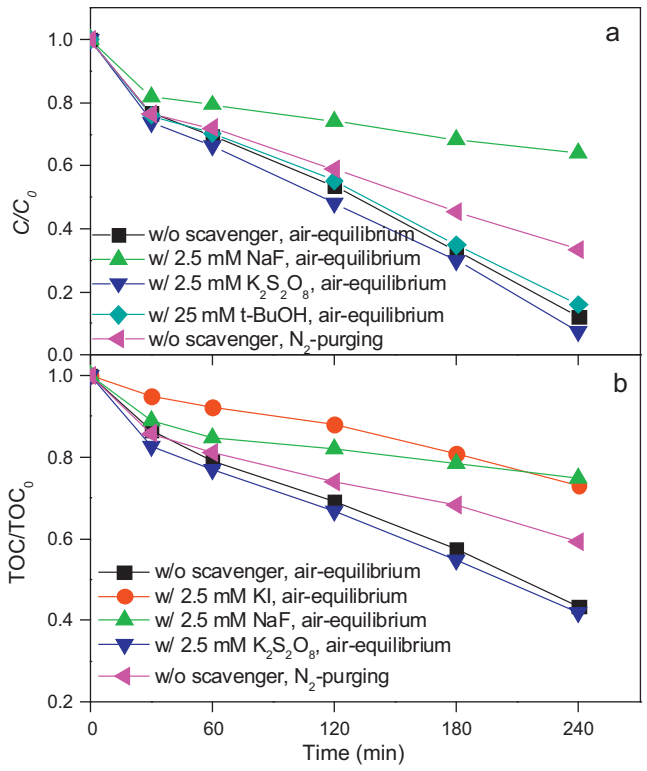

Fig. 7. Comparison of the 2-CP removal (a) and TOC reduction (b) in the presence of SIT_5-400 under visible light irradiation with scavengers in an air equilibrium system, without scavengers in an air equilibrium system, and without scavengers in a N_2-purged system. Initial 2-CP concentration, 0.25 mM; catalyst dosage, 1.0 g L^{-1}; reaction temperature, 22 °C.

the HO• cannot be responsible for 2-CP removal since the addition of 25 mM *t*-BuOH did not reduce the rate of 2-CP removal. From this experiment, along with the test in the presence of KI, we concluded that the h_{vb}^+ over the photocatalyst was promoted as responsible for the degradation of 2-CP.The role of oxygen is commonly regarded as a CB electron scavenger to prevent the recombination of electron–hole pairs [43,45,47,48].

$$e_{cb}^- + O_2 \rightarrow O_2^{-\bullet}$$

$$O_2^{-\bullet} + e_{cb}^-(+2H^+) \rightarrow H_2O_2$$

$$H_2O_2 + O_2^{-\bullet} \rightarrow HO^\bullet + OH^- + O_2$$

$$H_2O_2 + h\nu \rightarrow 2HO^\bullet$$

The solution with SIT_5-400 suspensions purged with N_2, can decrease the dissolved oxygen level from 0.15 mM to 0.01 mM. In this case, a significantly lower rate of 2-CP degradation than that in the air-equilibrated solution was observed. This result corroborated the importance of oxygen to the removal of 2-CP as the acceptor of photoelectrons, suppressing the recombination of electron and hole pairs. A further experiment looking at 2-CP removal was done using the more efficient e_{cb}^- acceptor $K_2S_2O_8$ [49].

$$S_2O_8^{2-} + e_{cb}^- \rightarrow SO_4^{-\bullet} + SO_4^{2-}$$

$$SO_4^{-\bullet} + e_{cb}^- \rightarrow SO_4^{2-}$$

$$SO_4^{-\bullet} + H_2O \rightarrow OH^\bullet + SO_4^{2-} + H^+$$

We found that the photocatalytic degradation rate was not restrained by the addition of 2.5 mM $K_2S_2O_8$, suggesting that the

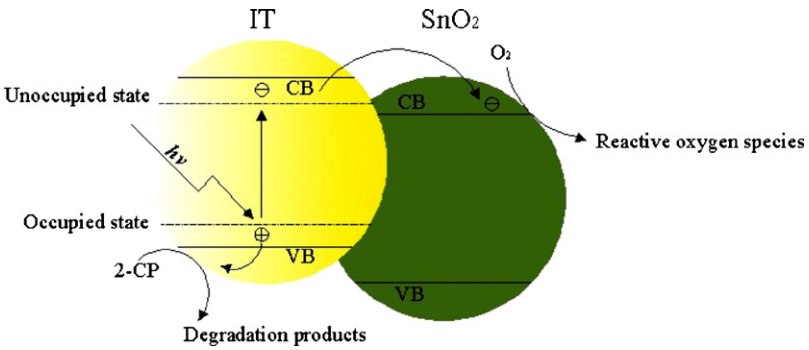

Scheme 1. Schematic diagram of the charge-transfer process.

electronic pathway is insignificant for the photodegradation of 2-CP. Instead, the presence of $K_2S_2O_8$ in SIT_5-400 suspensions promoted slightly the reaction rate because the $S_2O_8^{2-}$ can trap e_{cb}^- to leave more h_{vb}^+ available for photo-reaction [50].Combining the above, a mechanistic scheme was proposed to serve as a working hypothesis for the catalytic paths (Scheme 1). The whole process consists of exciton formation, exciton dissociation into free carriers, the transfer of free carriers to the surface, and the generation of reactive oxygen species. During the photocatalytic process under visible light, the absorption of a photon by IT leads to the promotion of an electron from the occupied state of I–O–Ti to an unoccupied state of I–O–I [15], and then the electron is transferred to the conduction band of SnO_2. In this way, the CB of SnO_2 acts as a sink for photogenerated electrons reacting with oxygen to generate reactive oxygen species. The photogenerated holes move in the opposite direction, accumulating in the VB of the IT and reacting with 2-CP to generate degradation products.

4. Conclusion

Overall experimental results indicate that using SIT photocatalysis to degrade the 2-CP is a viable treatment alternative. The phase structure, surface area, morphology and absorption wavelength range of the catalysts were affected by the Sn/Ti ratio and calcination temperature. The SIT_5-400 sample was photocatalytically superior to the corresponding IT in the process of 2-CP degradation under visible light irradiation. The surface mixing of SnO_2 to IT served as a sink for the photogenerated electrons and thus decreased the electron–hole pair recombination rate. The photogenerated holes accumulate in the VB of the IT reacting with 2-CP and subsequently improved the PA of the TiO_2. We believe that with further investigation and improvement this photocatalyst will be worthy of application in the degradation of other organic contaminants in wastewater, utilizing solar energy efficiently.

Acknowledgments

This work was supported by the National Natural Science Foundation of China (grant nos. 20977086 and 21076196), the National Basic Research Program of China (grant no. 2009CB421603), and the Zhejiang Provincial Natural Science Foundation of China (grant nos. Z5080207 and Y5100310).

References

[1] A. Fujishima, K. Honda, Electrochemical photolysis of water at a semiconductor electrode, Nature 238 (1972) 37–38.
[2] C.D. Jaeger, A.J. Bard, Spin trapping and electron spin resonance detection of radical intermediates in the photodecomposition of water at TiO_2 particulate systems, J. Phys. Chem. 83 (1979) 3146–3152.
[3] M.R. Hoffmann, S.T. Martin, W.Y. Choi, D.W. Bahnemannt, Environmental applications of semiconductor photocatalysis, Chem. Rev. 95 (1995) 69–96.
[4] A. Fujishima, X.T. Zhang, D.A. Tryk, TiO_2 photocatalysis and related surface phenomena, Surf. Sci. Rep. 63 (2008) 515–582.
[5] Z.Q. He, X. Xu, S. Song, L. Xie, J.J. Tu, J.M. Chen, B. Yan, A visible light-driven titanium dioxide photocatalyst codoped with lanthanum and iodine: an application in the degradation of oxalic acid, J. Phys. Chem. C 112 (2008) 16431–16437.
[6] W. Balcerski, S.Y. Ryu, M.R. Hoffmann, Visible-light photoactivity of nitrogen-doped TiO_2: photo-oxidation of HCO_2H to CO_2 and H_2O, J. Phys. Chem. C 111 (2007) 15357–15362.
[7] G.T. Li, J.H. Qu, X.W. Zhang, H.J. Liu, H.N. Liu, Electrochemically assisted photocatalytic degradation of Orange II: Influence of initial pH values, J. Mol. Catal. A: Chem. 259 (2006) 238–244.
[8] O. Carp, C.L. Huisman, A. Reller, Photoinduced reactivity of titanium dioxide, Prog. Solid State Chem. 32 (2004) 33–177.
[9] L.C. Chen, F.R. Tsai, S.H. Fang, Y.C. Ho, Properties of sol–gel SnO_2/TiO_2 electrodes and their photoelectrocatalytic activities under UV and visible light illumination, Electrochim. Acta 54 (2009) 1304–1311.
[10] P.A. Carneiro, M.E. Osugi, J.J. Sene, M.A. Anderson, M.V.B. Zanoni, Evaluation of color removal and degradation of a reactive textile azo dye on nanoporous TiO_2 thin-film electrodes, Electrochim. Acta 49 (2004) 3807–3820.
[11] X.T. Hong, Z.P. Wang, W.M. Cai, F. Lu, J. Zhang, Y.Z. Yang, N. Ma, Y.J. Liu, Visible-light-activated nanoparticle photocatalyst of iodine-doped titanium dioxide, Chem. Mater. 17 (2005) 1548–1552.
[12] G. Liu, Z.G. Chen, C.L. Dong, Y.N. Zhao, F. Li, G.Q. Lu, H.M. Cheng, Visible light photocatalyst: iodine-doped mesoporous titania with a bicrystalline framework, J. Phys. Chem. B 110 (2006) 20823–20828.
[13] S. Tojo, T. Tachikawa, M. Fujitsuka, T. Majima, Iodine-doped TiO_2 photocatalysts: correlation between band structure and mechanism, J. Phys. Chem. C 112 (2008) 14948–14954.
[14] W.Y. Su, Y.F. Zhang, Z.H. Li, L. Wu, X.X. Wang, J.Q. Li, X.Z. Fu, Multivalency iodine doped TiO_2: preparation, characterization, theoretical studies, and visible-light photocatalysis, Langmuir 24 (2008) 3422–3428.
[15] G. Liu, C.H. Sun, X.X. Yan, L. Cheng, Z.G. Chen, X.W. Wang, L.Z. Wang, S.C. Smith, G.Q. Lu, H.M. Cheng, Iodine doped anatase TiO_2 photocatalyst with ultra-long visible light response: correlation between geometric/electronic structures and mechanisms, J. Mater. Chem. 19 (2009) 2822–2829.
[16] R. Sasikala, A. Shirole, V. Sudarsan, T. Sakuntala, C. Sudakar, R. Naik, S.R. Bharadwaj, Highly dispersed phase of SnO_2 on TiO_2 nanoparticles synthesized by polyol-mediated route: photocatalytic activity for hydrogen generation, Int. J. Hydrogen Energ. 34 (2009) 3621–3630.
[17] K. Zakrzewska, M. Radecka, TiO_2–SnO_2 system for gas sensing – photodegradation of organic contaminants, Thin Solid Films 515 (2007) 8332–8338.
[18] S.F. Chen, L. Chen, S. Gao, G.Y. Cao, The preparation of coupled SnO_2/TiO_2 photocatalyst by ball milling, Mater. Chem. Phys. 98 (2006) 116–120.
[19] L.R. Hou, C.Z. Yuan, Y. Peng, Synthesis and photocatalytic property of SnO_2/TiO_2 nanotubes composites, J. Hazard. Mater. B 139 (2007) 310–315.
[20] K. Vinodgopal, P.V. Kamat, Enhanced rates of photocatalytic degradation of an azo dye using SnO_2/TiO_2 coupled semiconductor thin films, Environ. Sci. Technol. 29 (1995) 841–845.
[21] H. Tada, A. Hattori, Y. Tokihisa, K. Imai, N. Tohge, S. Ito, A patterned-TiO_2/SnO_2 bilayer type photocatalyst, J. Phys. Chem. B 104 (2000) 4585–4587.
[22] J. Ananpattarachai, P. Kajitvichyanukul, S. Seraphin, Visible light absorption ability and photocatalytic oxidation activity of various interstitial N-doped TiO_2 prepared from different nitrogen dopants, J. Hazard. Mater. 168 (2009) 253–261.
[23] T. Putta, M.C. Lu, J. Anotai, Characterization and activity of visible-light driven TiO_2 photocatalyst doped with tungsten, Water Sci. Technol. 62 (2010) 2128–2133.
[24] Y. Ku, Y.C. Li, W.Y. Wang, C.M. Ma, Y.C. Chou, Effect of platinum on the photocatalytic decomposition of 2-chlorophenol in aqueous solution by UV/TiO_2, J. Chin. Inst. Eng. 33 (2010) 591–596.
[25] S.H. Song, M. Kang, Decomposition of 2-chlorophenol using a tourmaline – photocatalytic system, J. Ind. Eng. Chem. 14 (2008) 785–791.
[26] K. Mogyorósi, A. Farkas, I. Dékány, I. Ilisz, A. Dombi, TiO_2-based photocatalytic degradation of 2-chlorophenol adsorbed on hydrophobic clay, Environ. Sci. Technol. 36 (2002) 3618–3624.

[27] M.A. Barakat, H. Schaeffer, G. Hayes, S. Ismat-Shah, Photocatalytic degradation of 2-chlorophenol by co-doped TiO_2 nanoparticles, Appl. Catal. B-Environ. 57 (2005) 23–30.
[28] D. Gryglik, J.S. Miller, S. Ledakowicz, Singlet molecular oxygen application for 2-chlorophenol removal, J. Hazard. Mater. 146 (2007) 502–507.
[29] M.H. Zhou, J.G. Yu, S.W. Liu, P.C. Zhai, L. Jiang, Effects of calcination temperatures on photocatalytic activity of SnO_2/TiO_2 composite films prepared by an EPD method, J. Hazard. Mater. 154 (2008) 1141–1148.
[30] Q.H. Shen, H. Yang, Q. Xu, Y. Zhu, R. Hao, In-situ preparation of TiO_2/SnO_2 nanocrystalline sol for photocatalysis, Mater. Lett. 64 (2010) 442–444.
[31] Q.J. Liu, X.H. Wu, B.L. Wang, Q. Liu, Preparation and super-hydrophilic properties of TiO_2/SnO_2 composite thin films, Mater. Res. Bull. 37 (2002) 2255–2262.
[32] L.D. Gelb, K.E. Gubbins, R. Radhakrishnan, M. Sliwinska-Bartkowiak, Phase separation in confined systems, Rep. Prog. Phys. 62 (1999) 1573–1659.
[33] S. Takenaka, R. Takahashi, S. Sato, T. Sodesawa, F. Matsumoto, S. Yoshida, Pore size control of mesoporous SnO_2 prepared by using stearic acid, Micropor. Mesopor. Mater. 59 (2003) 123–131.
[34] T.Y. Peng, D. Zhao, K. Dai, W. Shi, K. Hirao, Synthesis of titanium dioxide nanoparticles with mesoporous anatase wall and high photocatalytic activity, J. Phys. Chem. B 109 (2005) 4947–4952.
[35] Z. Ibrahim, Z. Othaman, A. Karim, M. Mustamam, D. Holland, X-ray photoemission spectroscopy (XPS) analysis on platinum doped stannic oxide ceramic, Solid State Sci. Technol. 15 (2007) 65–73.
[36] S.F. Chen, W. Zhao, W. Liu, S.J. Zhang, Preparation, characterization and activity evaluation of p-n junction photocatalyst p-$CaFe_2O_4$/n-Ag_3VO_4 under visible light irradiation, Appl. Surf. Sci. 255 (2008) 2478–2484.
[37] E.M. El-Maghraby, Effect of Sn ratio on the photocatalytic degradation of methylene blue and soot of ink by TiO_2–SnO_2 nanostructured thin films, Phys. B 405 (2010) 2385–2389.
[38] Y.D. Hou, X.C. Wang, L. Wu, X.F. Chen, Z.X. Ding, X.X. Wang, X.Z. Fu, N-doped SiO_2/TiO_2 mesoporous nanoparticles with enhanced photocatalytic activity under visible-light irradiation, Chemosphere 72 (2008) 414–421.
[39] J.T. Tian, J.F. Wang, J.H. Dai, X. Wang, Y.S. Yin, N-doped TiO_2/ZnO composite powder and its photocatalytic performance for degradation of methyl orange, Surf. Coat. Technol. 204 (2009) 723–730.
[40] S. Song, J.J. Tu, Z.Q. He, F.Y. Hong, W.P. Liu, J.M. Chen, Visible light-driven iodine-doped titanium dioxide nanotubes prepared by hydrothermal process and post-calcination, Appl. Catal. A Gen. 378 (2010) 169–174.
[41] Z.Q. He, L. Xie, J.J. Tu, S. Song, W.P. Liu, Z.W. Liu, J.Q. Fan, Q. Liu, J.M. Chen, Visible light-induced degradation of phenol over iodine-doped titanium dioxide modified with platinum: role of platinum and the reaction mechanism, J. Phys. Chem. C 114 (2010) 526–532.
[42] C. Minero, G. Mariella, V. Maurino, D. Vione, E. Pelizzetti, Photocatalytic transformation of organic compounds in the presence of inorganic ions 2. Competitive reactions of phenol and alcohols on a titanium dioxide-fluoride system, Langmuir 16 (2000) 8964–8972.
[43] Y.X. Chen, S.Y. Yang, K. Wang, L.P. Lou, Role of primary active species and TiO_2 surface characteristic in UV-illuminated photodegradation of Acid Orange 7, J. Photochem. Photobiol A Chem. 172 (2005) 47–54.
[44] S. Song, L.J. Xu, Z.Q. He, J.M. Chen, X.Z. Xiao, B. Yan, Mechanism of the photocatalytic degradation of C.I. Reactive Black 5 at pH 12.0 using $SrTiO_3/CeO_2$ as the catalyst, Environ. Sci. Technol. 41 (2007) 5846–5853.
[45] S.T. Martin, A.T. Lee, M.R. Hoffmann, Chemical mechanism of inorganic oxidants in the TiO_2/UV Process: increased rates of degradation of chlorinated hydrocarbons, Environ. Sci. Technol. 29 (1995) 2567–2573.
[46] T. Torii, K. Yasui, K. Yasuda, Y. Iida, T. Tuziuti, T. Suzuki, M. Nakamura, Generation and consumption rates of OH radicals in sonochemical reactions, Res. Chem. Intermed. 30 (2004) 713–721.
[47] Y. Ou, J.D. Lin, H.M. Zou, D.W. Liao, Effects of surface modification of TiO_2 with ascorbic acid on photocatalytic decolorization of an Azo dye reactions and mechanisms, J. Mol. Catal. A: Chem. 241 (2005) 59–64.
[48] K. Okamoto, Y. Yamamoto, H. Tanaka, M. Tanaka, A. Itaya, Heterogeneous photocatalytic decomposition of phenol over TiO_2 powder, Bull. Chem. Soc. Jpn. 58 (1985) 2015–2022.
[49] M. Muruganandham, N. Shobana, M. Swaminathan, Optimization of solar photocatalytic degradation conditions of Reactive Yellow 14 azo dye in aqueous TiO_2, J. Mol. Catal. A: Chem. 246 (2006) 154–161.
[50] Z.Q. He, L. Xie, S. Song, C. Wang, J.J. Tu, F.Y. Hong, Q. Liu, J.M. Chen, X.H. Xu, The impact of silver modification on the catalytic activity of iodine-doped titania for *p*-chlorophenol degradation under visible-light irradiation, J. Mol. Catal. A: Chem. 319 (2010) 78–84.